

## SUPERSONIC DOWNFLOWS AT THE UMBRA-PENUMBRA BOUNDARY OF SUNSPOTS

ROHAN E. LOUIS<sup>1</sup>, LUIS R. BELLOT RUBIO<sup>2</sup>, SHIBU K. MATHEW<sup>1</sup> AND P. VENKATAKRISHNAN<sup>1</sup>

*Draft version October 31, 2018*

### ABSTRACT

High resolution spectropolarimetric observations of 3 sunspots taken with *Hinode* demonstrate the existence of supersonic downflows at or close to the umbra-penumbra boundary which have not been reported before. These downflows are confined to large patches, usually encompassing bright penumbral filaments, and have lifetimes of more than 14 hr. The presence of strong downflows in the center-side penumbra near the umbra rules out an association with the Evershed flow. Chromospheric filtergrams acquired close to the time of the spectropolarimetric measurements show large, strong, and long-lived brightenings in the neighborhood of the downflows. The photospheric intensity also exhibit persistent brightenings comparable to the quiet Sun. Interestingly, the orientation of the penumbral filaments at the site of the downflows is similar to that resulting from the reconnection process described by Ryutova et al. (2008a). The existence of such downflows in the inner penumbra represents a challenge for numerical models of sunspots because they have to explain them in terms of physical processes likely affecting the chromosphere.

*Subject headings:* Sun: magnetic fields—sunspots—techniques: polarimetric

### 1. INTRODUCTION

The Evershed flow (EF; Evershed 1909) is a well known phenomenon associated with the filamentary structure of sunspot penumbrae (Solanki 2003, and references therein). The EF is observed as a shift of the spectral lines, due to a nearly horizontal, radial outflow of plasma that starts as upflows in the deep layers of the inner penumbra (Bellot Rubio et al. 2006; Rimmele & Marino 2006; Franz & Schlichenmaier 2009) and ends in a ring of downflow channels in the mid and outer penumbra (Westendorp Plaza et al. 1997; Schlichenmaier & Schmidt 1999; Mathew et al. 2003; Bellot Rubio et al. 2004; Borrero et al. 2005). The weak Evershed upflows in the inner penumbra are associated with bright penumbral grains that migrate towards the umbra-penumbra boundary with speeds of  $\approx 1 \text{ km s}^{-1}$  (Rimmele & Marino 2006) while individual velocity packets are observed to propagate towards the periphery of the sunspot with velocities of 2–5.5  $\text{km s}^{-1}$  (Rimmele 1994) and vary on a time scale of 10–20 min (Rimmele 1994; Shine et al. 1994; Rouppe van der Voort 2003; Cabrera Solana et al. 2007).

Apart from the EF, the penumbra harbors other types of mass motions. Recent *Hinode* observations by Katsukawa & Jurčák (2010) have revealed localized downflows that do not appear to be related to the EF. These downflows, with velocities of up to 1  $\text{km s}^{-1}$ , have a typical size of  $0''.5$ . Some of them are seen to be co-spatial with Ca brightenings in the chromosphere. Katsukawa & Jurčák (2010) pointed out that the downflowing areas have the same polarity as the parent sunspot and are unlikely to be the Evershed mass returning to the photosphere, which sometimes happens well within the penumbra (Bellot Rubio et al. 2004, 2007; Sainz Dalda & Bellot Rubio 2008).

In this paper we describe a new type of downflows that are observed close to or at the umbra-penumbra boundary and show supersonic velocities. They have the same polarity as the spot, occupy an area larger than 1.5  $\text{arcsec}^2$ , and occur along bright penumbral filaments. These properties are different from those of the radial Evershed flow and the downflows reported by Katsukawa & Jurčák (2010), which indicates a different physical origin. The strong downflows we have detected possibly represent dynamic processes occurring in the penumbra whose manifestation is also seen in the overlying chromosphere.

### 2. OBSERVATIONS

Spectro-polarimetric observations of NOAA AR 10923, 10953 and 11029 were carried out using the Solar Optical Telescope (SOT; Tsuneta et al. 2008) on board *Hinode* (Kosugi et al. 2007), on 2006 November 10, 2007 May 1 and 2009 October 27 respectively. The sunspots were located at heliocentric angles of  $50^\circ$ ,  $8^\circ$  and  $43^\circ$  as shown in Figure 1. They were mapped by the spectro-polarimeter (SP; Lites et al. 2001; Ichimoto et al. 2008) from 16:01 UT to 17:25 UT, 21:00 UT to 22:24 UT and 14:45 UT to 15:15 UT respectively. At each slit position the four Stokes profiles of the neutral iron lines at 630 nm were recorded with a spectral sampling of 21.55 mÅ. While the first two ARs were scanned in the normal mapping mode with an exposure time of 4.8 s and a pixel size of  $0''.16$ , the fast mode was used to observe AR 11029 with exposure times of 1.6 s and a pixel size of  $0''.32$ . The measurements were corrected for dark current, flat field, thermal flexures, and instrumental polarization using the SolarSoft package. The zero point of the velocity scale was set at the line core position of the average quiet Sun profile, determined considering all the pixels with polarization signals smaller than three times the noise level.

G-band and Ca II H filtergrams acquired by the Broadband Filter Imager (BFI) close to the SP scans were also employed. The filtergrams had a sampling of  $0''.055$ ,  $0''.11$  and  $0''.11$  and a cadence of 30 s, 1 min and 5 min

Electronic address: eugene@prl.res.in

<sup>1</sup> Udaipur Solar Observatory, Physical Research Laboratory Dewali, Badi Road, Udaipur, Rajasthan - 313004, India

<sup>2</sup> Instituto de Astrofísica de Andalucía (CSIC), Apartado de Correos 3004, 18080 Granada, Spain

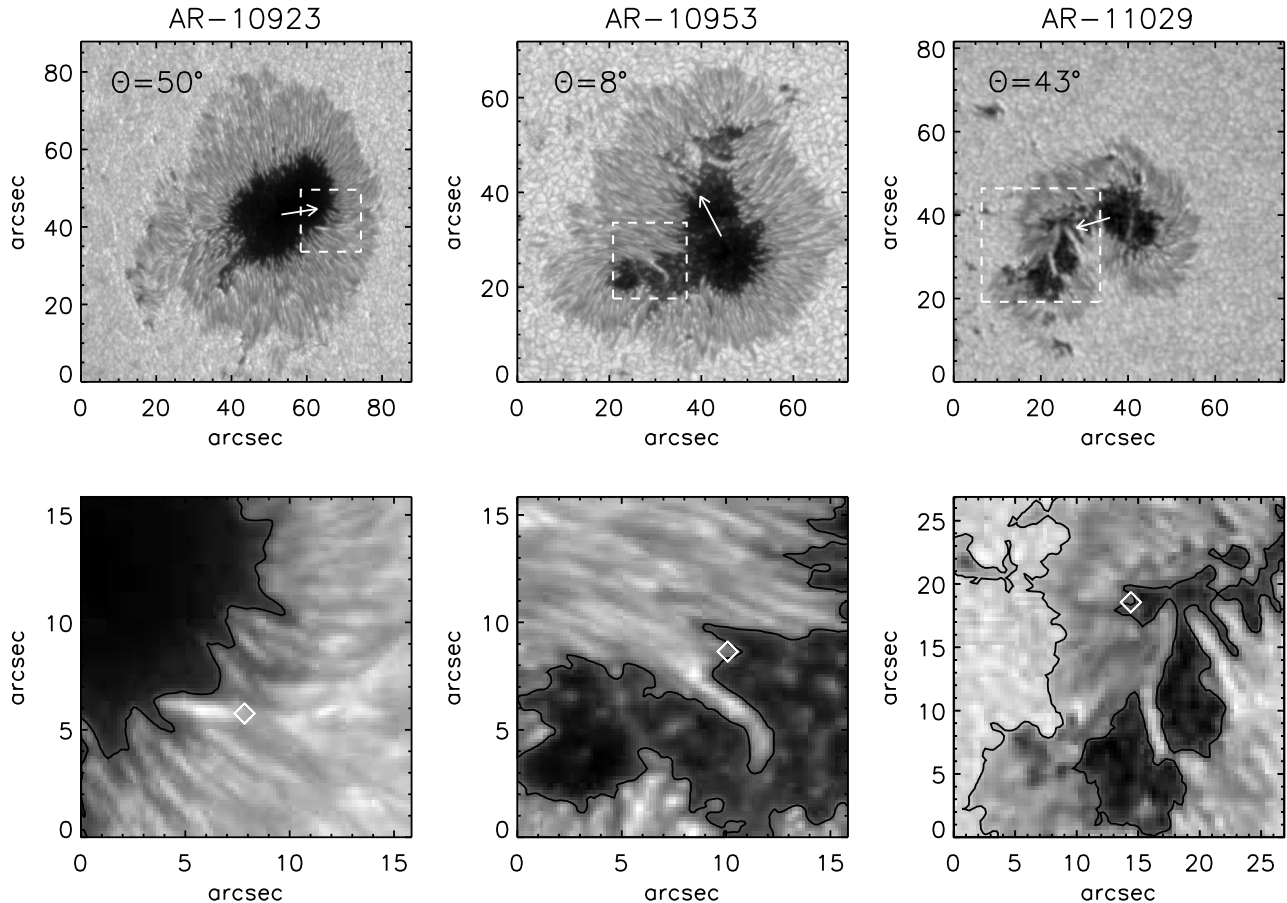


FIG. 1.— Sunspots studied in this paper. **Top:** continuum intensity maps constructed from the SP scans. The arrow points to disc center. **Bottom:** Enlargement of the regions marked by white-dashed squares in the top panels. The diamonds represent the pixels whose Stokes profiles are shown in Figure 3.

respectively. These data were recorded from 13:00 to 14:00 UT, 20:00 to 20:58 UT and 14:00 to 15:55 UT respectively. The Ca images were obtained simultaneously with the SP scans for AR 11029 while the time separation between the Ca data set and the Stokes spectra for AR 10923 and 10953 were 3 hr and 1 hr respectively. The filtergrams were flat fielded and corrected for dark current and bad pixels. The analysis presented in this paper pertains to a small sub-region of the center-side penumbra as shown in the bottom panels of Figure 1.

### 3. RESULTS

#### 3.1. *Supersonic Downflows*

##### 3.1.1. *Far Wing Magnetograms*

To identify sites with large velocities we construct magnetograms in the far blue and red wings of the Stokes V profile,  $\pm 34.4$  pm from the center of the 630.25 nm line. This method was applied by Ichimoto et al. (2007) to locate the sources and sinks of the Evershed flow. The sunspots of all 3 ARs have negative polarity and the sign of the red wing magnetograms has been reversed to match that of the blue wing.

The top and middle panels of Figure 2 display the red and blue wing magnetograms, both of which have been scaled identically. As is evident, the red wing magnetograms show very strong signals while their blue counterparts do not. In AR 10923 we can see two distinct fila-

mentary structures very close to one another, with Stokes V signals of about 9% (Figure 2, top left panel). The blue magnetogram of the same sub-region shows a similar (but weaker) isolated filamentary structure that lies very close to the umbra-penumbra boundary. Part of this feature is observed also in the red wing magnetogram (at the position of the diamond marked in Figure 2), which is indicative of strong magnetic fields. The extended feature is also co-spatial with an extremely bright filament in the corresponding continuum image (Figure 1).

Two patches of very strong V signal, separated by  $\sim 3''$ , are observed in the red wing magnetogram of AR 10953 with one of them lying at the umbra-penumbra boundary. In AR 11029 there are two extended regions near the edge of the umbra, with strong V signals of up to 20% of the continuum intensity.

##### 3.1.2. *LOS Velocities from SIR*

While the far wing magnetograms are useful to locate pixels with large velocities, the actual magnitude cannot be quantified merely from the strength of the signals. In order to estimate the range of velocities present in those pixels, the observed Stokes profiles were subject to an inversion using the SIR code (Stokes Inversion based on Response Functions; Ruiz Cobo & del Toro Iniesta 1992). The simplest model atmosphere was assumed wherein the vector magnetic field (field strength, inclination and azimuth) and LOS velocity were kept constant with

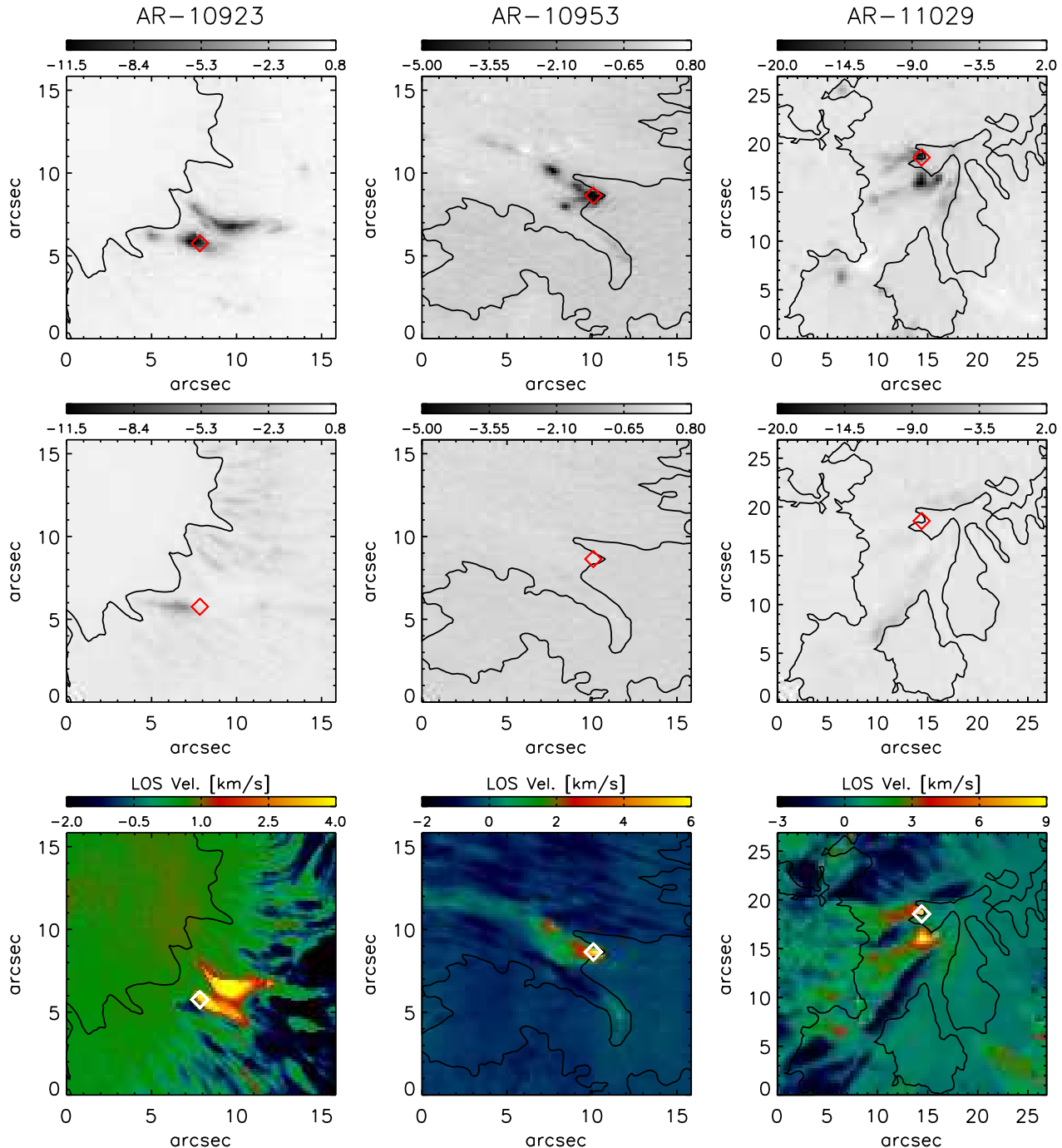


FIG. 2.— **Top:** Red wing magnetograms constructed at  $+34.4$  pm from the  $6302.5\text{\AA}$  line for NOAA ARs 10923, 10953 and 11029 (from left to right respectively). The sign of the signal has been reversed. **Center:** Blue wing magnetograms constructed at  $-34.4$  pm from the  $6302.5\text{\AA}$  line. The numbers in the gray scale color bars are expressed in per cent. **Bottom:** LOS velocities derived from the SIR inversion. Positive velocities indicate downflows. The maps have been scaled individually. The diamonds represent pixels located in strong downflowing regions; their Stokes profiles are displayed in Figure 3.

height, while the temperature was perturbed with 2 nodes. The inversions also retrieved height-independent micro- and macro-turbulent velocities as well as the fraction of stray light in each pixel.

The lower panels of Figure 2 depict the resulting LOS velocities for the 3 ARs. These values must be regarded as approximate since large gradients of the atmospheric parameters may exist along the LOS. The structure of the downflows is remarkably, but not surprisingly, similar to that seen in the far red wing magnetograms. While strong downflows of  $\sim 5$  km  $\text{s}^{-1}$  are observed in AR

10923, one finds velocities of around 6 km  $\text{s}^{-1}$  and 10 km  $\text{s}^{-1}$  in ARs 10953 and 11029 respectively. The strong downflowing zones are surrounded by upflows which can be identified with the Evershed flow.

The majority of the Stokes V profile emerging from the downflows exhibit a satellite or even an additional red lobe. The Stokes I profiles also have highly inclined red wings, as illustrated in the top row of Figure 3 for the pixels marked with diamonds in Figure 2. In AR 11029, some of the downflows exhibit strongly redshifted V profiles with large area asymmetries (bottom row of

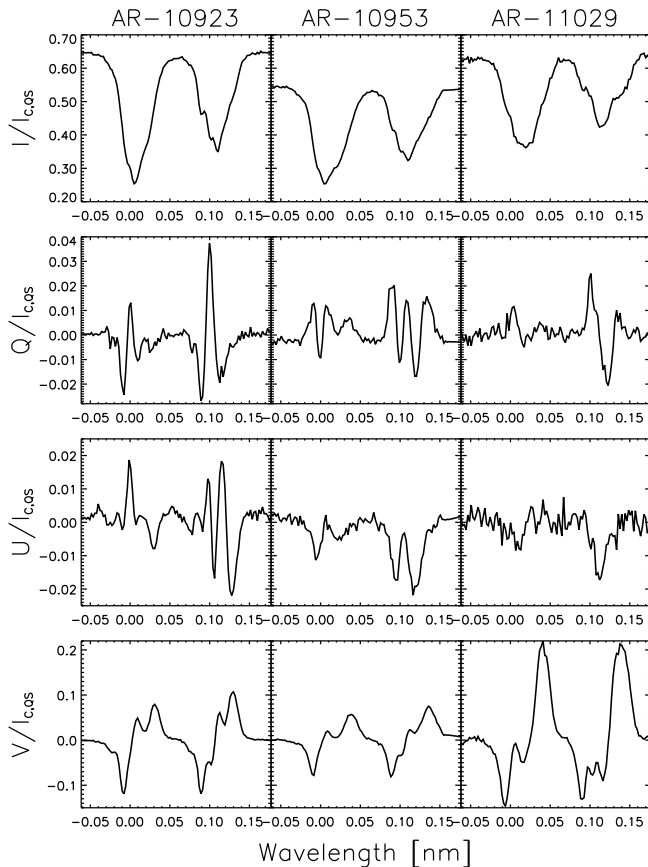


FIG. 3.— Stokes profiles corresponding to the pixels marked in Figures 1 and 2.

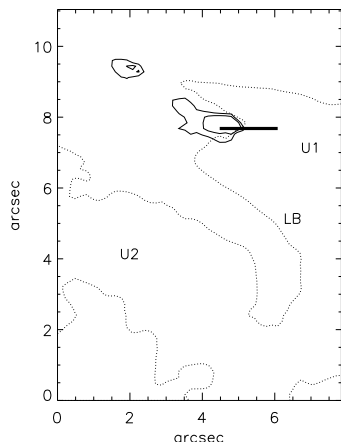


FIG. 4.— Continuum intensity contour of AR 10953 (black dotted lines). Black solid contours mark LOS velocities of 2.5 and 4 km s<sup>-1</sup>. The thick line represents a cut across the strong downflows at the umbra-penumbra boundary. The distance along the slit increases from left to right with the umbra-penumbra boundary being zero. Pixels to the left are negative. U1, U2 - umbrae; LB - light bridge.

Figure 3). Upflows of about 2 km s<sup>-1</sup> corresponding to the EF are seen adjacent to the strong downflowing patches in all 3 ARs.

Figure 4 shows a cut passing through the strong downflowing patch located at the umbra-penumbra boundary of AR 10953. The variation of the Stokes profiles along this cut is displayed in Figure 5 (black lines). At the umbral edge and to the right, one observes a dis-

tinct reduction in the continuum intensity. To the left of the umbra-penumbra boundary, the Stokes V profile has two distinct red lobes while the  $I$  profile exhibits highly inclined red wings. With five lobes, the Stokes Q profile is very asymmetric, 0'32 beyond the edge of the umbra. The anomalous profiles lying to the left of the umbra-penumbra boundary were inverted using a 2 component atmosphere and setting all parameters, except the temperature, to be constant with height in order to estimate the physical parameters more precisely. The highly inclined red wings of the Stokes  $I$  profiles as well as the double-red-lobed V profiles are well reproduced by the simple two-component atmosphere (lines with black filled circles in Figure 5). The transition from supersonic to nearly zero velocities along the cut can be seen in Figure 6, which shows that very large velocities nearly twice the sound speed occur adjacent/close to the umbra-penumbra boundary and measure  $\approx 7.2$  km s<sup>-1</sup> at a distance of  $-0'64$ . At the umbral edge the faster component has a fill fraction of  $\approx 11\%$  which increases with distance and beyond  $-0'64$  fills more than 70% of the pixel. While the fast and slow components appear to differ by  $\approx 300$  G the uncertainties in the retrieved parameters suggest that the magnitudes are nearly the same. Both components have field strengths in excess of 2.2 kG. The average zenith angle in the umbra is  $\approx 143^\circ$  and changes from  $142 \pm 2^\circ$  at the umbra penumbra boundary to  $137 \pm 5^\circ$  at  $-0'96$  for the slow component. In comparison, the zenith angle of the fast component varies from  $150 \pm 11^\circ$  to  $124 \pm 4^\circ$  for the same spatial locations.

The typical area of one downflowing patch varies from 1.6 arcsec<sup>2</sup> for AR 10953 to as large as 6 arcsec<sup>2</sup> as observed in AR 11029. The two components could reside side-by-side in the same resolution element or could be stacked one on top of the other in the vertical direction. Regardless of the exact configuration, supersonic velocities exist in the presence of very strong magnetic fields. In addition, the polarity of the strong downflowing component is the same as that of the sunspot, which rules out the possibility of them being Evershed flows returning to the solar surface. The strong fields would also inhibit convection, hence the downflows appear to be unrelated to the Evershed phenomenon and are likely to be caused by an alternative mechanism.

### 3.2. Chromospheric Activity

Figure 7 depicts Ca II H filtergrams taken close to or during the time of the SP scans for the 3 ARs. In AR 10923, one can identify penumbral microjets (MJ) as well as brightness enhancements (BE) in the vicinity of the strong downflowing areas. The jet is the one shown in Figure 4 of Ryutova et al. (2008b). It is oriented nearly perpendicular to the filament, while the brightness enhancements appear as isolated zones on the filaments. These BEs are  $\sim 77\%$  brighter than the jets, which appear to be in the decay phase (Ryutova et al. 2008b). We will hereafter refer to the brightness enhancements and microjets as BEs and MJs respectively.

AR 10953 shows a very strong enhancement (BE) in between the two downflowing patches that is twice as intense as the neighbouring penumbra. Narrow, thread like structures (UT) of reduced intensity in the umbra are observed to connect to the nearby light bridge.

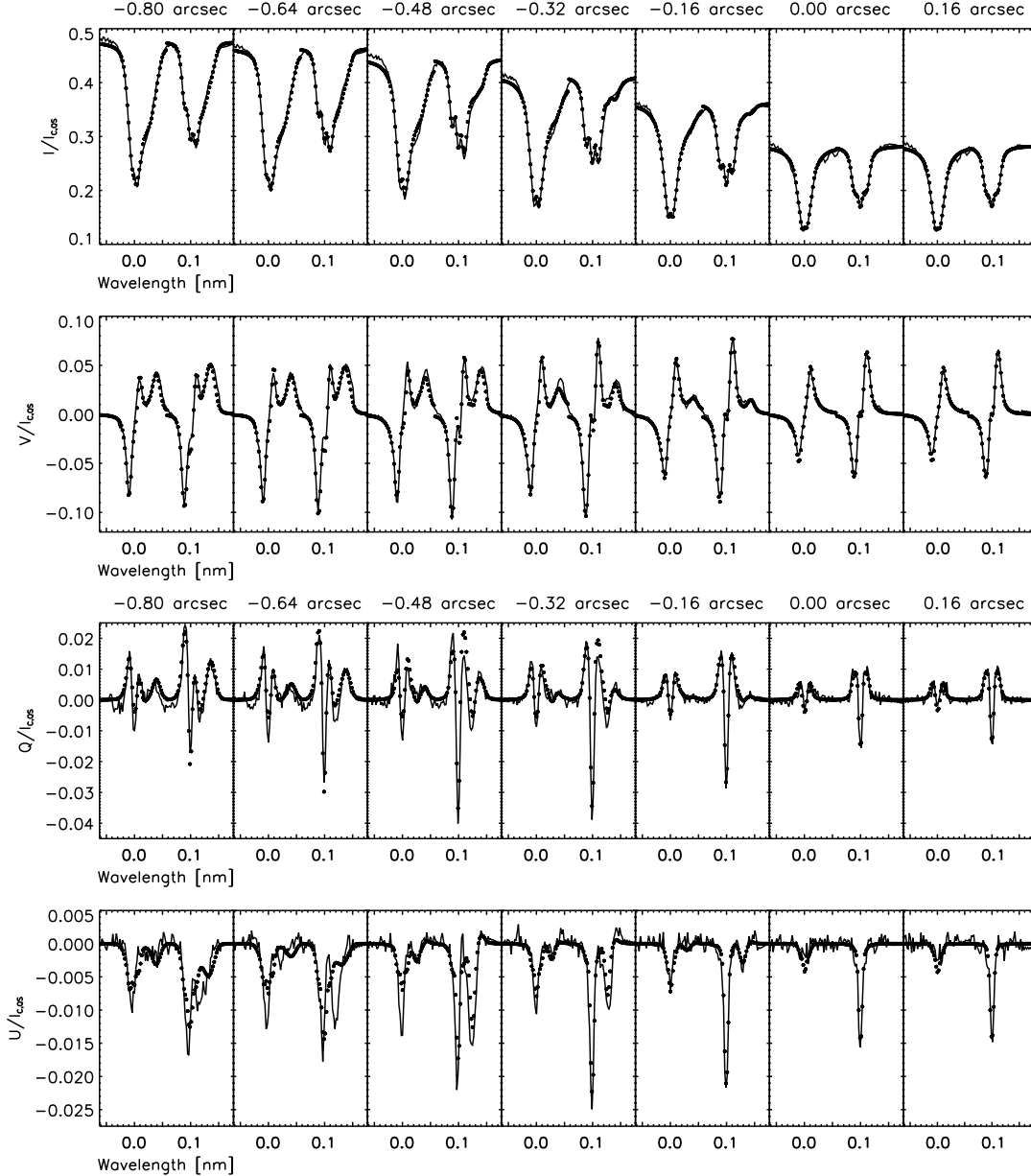


FIG. 5.— Observed (*black*) and best-fit (*black filled circles*) Stokes profiles along the cut marked in Figure 5. From top to bottom: Stokes I, V, Q and U.

Ca filtergrams with a cadence of 5 min taken simultaneously with the SP scan for AR 11029 exhibit an intense brightening at the umbra-penumbral boundary within one of the strong velocity patches. Even stronger brightenings are seen close to the outer penumbral boundary that lie at the rear end of the extended downflowing patch. A relatively weaker brightening is seen in the other velocity patch and occupies a much smaller area. These enhancements are  $\sim 50$  and 15% brighter than the adjacent penumbral filaments.

While Figure 7 shows single chromospheric snapshots highlighting the proximity of the downflows and the chromospheric enhancements, it does not provide information about whether the spatial correspondence between the two endures with time. In order to separate the short lived enhancements from the persistent ones, event maps were constructed from the time sequence of Ca filter-

grams acquired before/during the SP scans in the following manner. First, a small quiet Sun region was selected to determine the time averaged chromospheric intensity for each of the sequences. This value was then used to normalize the intensity of the individual filtergrams. A histogram of the intensities in the AR was derived to determine a suitable threshold value. From the trailing part of the histogram, threshold values of 0.9, 1.0 and 2.0 were chosen for the three ARs respectively. Using these values, a binary image was created for each individual image in the time sequence, where all pixels with an intensity above the threshold were set to one and the rest to zero. The binary maps were then added in time, yielding at the end, a map with pixels having values indicating the number of chromospheric events. The resulting event maps are shown in Figure 8.

The map constructed for AR 10923 displays two large

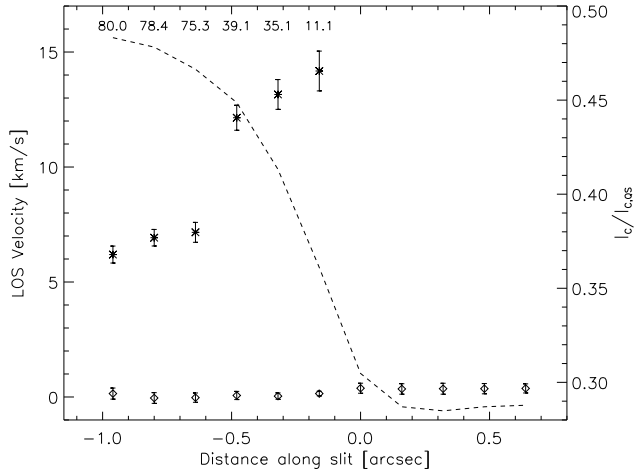


FIG. 6.— Variation of LOS velocity along the cut displayed in Figure 4, as resulting from an inversion of the observed Stokes profiles. The pixels left of the umbra-penumbra boundary were inverted using a two-component model atmosphere. The diamonds and asterisks represent the slow and fast component, respectively. The error bars correspond to  $\pm 1$  sigma. The dashed line shows the normalized continuum intensity along the slit. The numbers below the upper x-axis represent the filling fraction of the faster moving component.

patches on the penumbral filaments at the site of the downflows. They are labeled as BE in the top panel of Figure 7. The counts at those locations indicate that brightness enhancements persisted for nearly one-third of the 1 hr sequence. There are no obvious signatures of the MJ's, reflecting the transient nature and weakness of these events.

The strongest and long-lived chromospheric brightenings observed in AR 10953 are confined to a region between the two downflowing patches. AR 10953 produced several chromospheric enhancements from April 29 to the end of May 1 (Louis et al. 2008; Shimizu et al. 2009). Some of them were co-spatial with supersonic downflows observed in the light bridge nearly 10 hours earlier than the downflows reported here (Louis et al. 2009).

The bottom panel of Figure 8 shows the event map corresponding to AR 11029. The Ca filtergrams were acquired during the SP scan with a low cadence of 5 min. Here the strong and persistent enhancements at the umbra-penumbra boundary are co-spatial with the largest photospheric downflows. Similar brightenings are seen along the edges of the downflowing regions near the outer penumbral boundary. A relatively shorter but stronger event is observed in the other downflowing zone (black arrow in bottom panel of Figure 8). Several small C class flares were detected in NOAA AR 11029 during its passage on the solar disk from October 25 to October 28.

The chromospheric brightenings associated with strong downflowing patches near the umbra/penumbra boundary are more intense, persist in time and occupy a large area than the penumbral microjets discovered by Katsukawa et al. (2007). Microjets are transient events seen everywhere in the chromosphere of sunspot penumbrae, with lifetimes of 1 min or less. They show typical widths of 400 km and lengths varying from 1000 to 4000 km. In contrast, our events have areas of 1–2 arcsec<sup>2</sup> and appear as blobs or patches. Their lifetimes are sig-

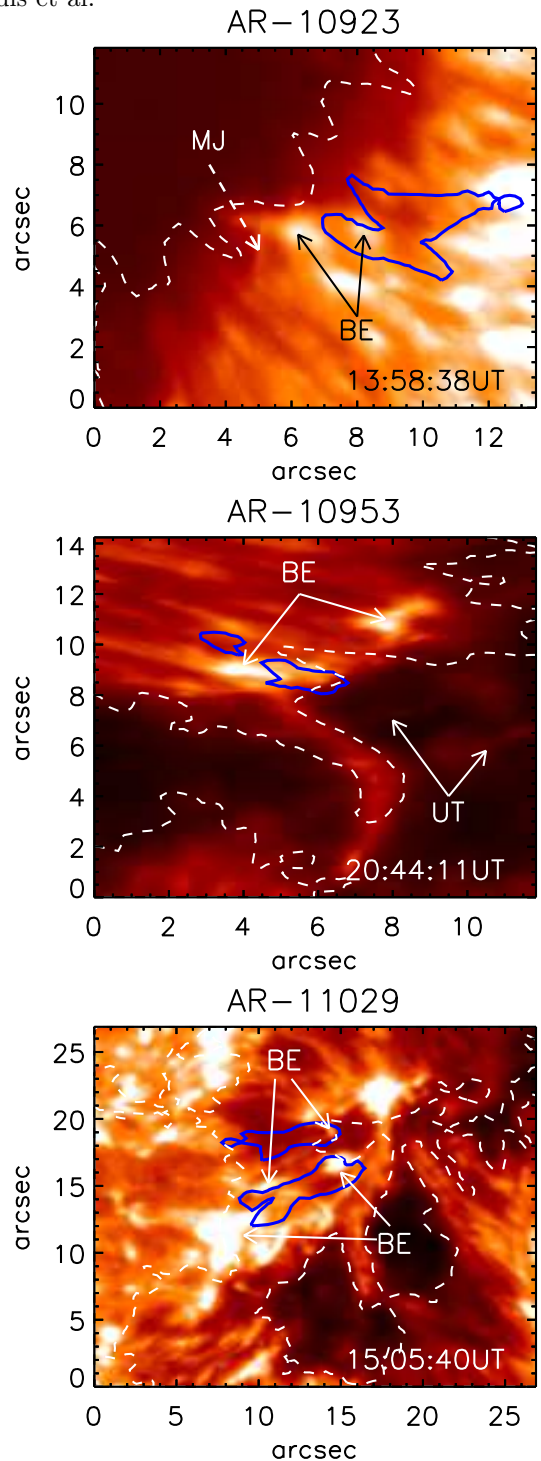


FIG. 7.— Ca II H filtergrams acquired close to the time of the SP scans. Blue contours of LOS velocity greater than  $2 \text{ km s}^{-1}$  have been overlaid on the filtergrams. The white dashed contour corresponds to the continuum intensity at 630 nm. BE - brightness enhancement; MJ - penumbral microjet; UT - bright umbral thread.

nificantly longer than 1 min.

### 3.3. Photospheric Brightness

In order to ascertain if the downflows are associated with long lived photospheric brightenings, G-band event maps were constructed as described in the previous section. The same procedure was adopted, setting threshold values of 0.85, 0.9 and 0.95 of the quiet Sun intensity for



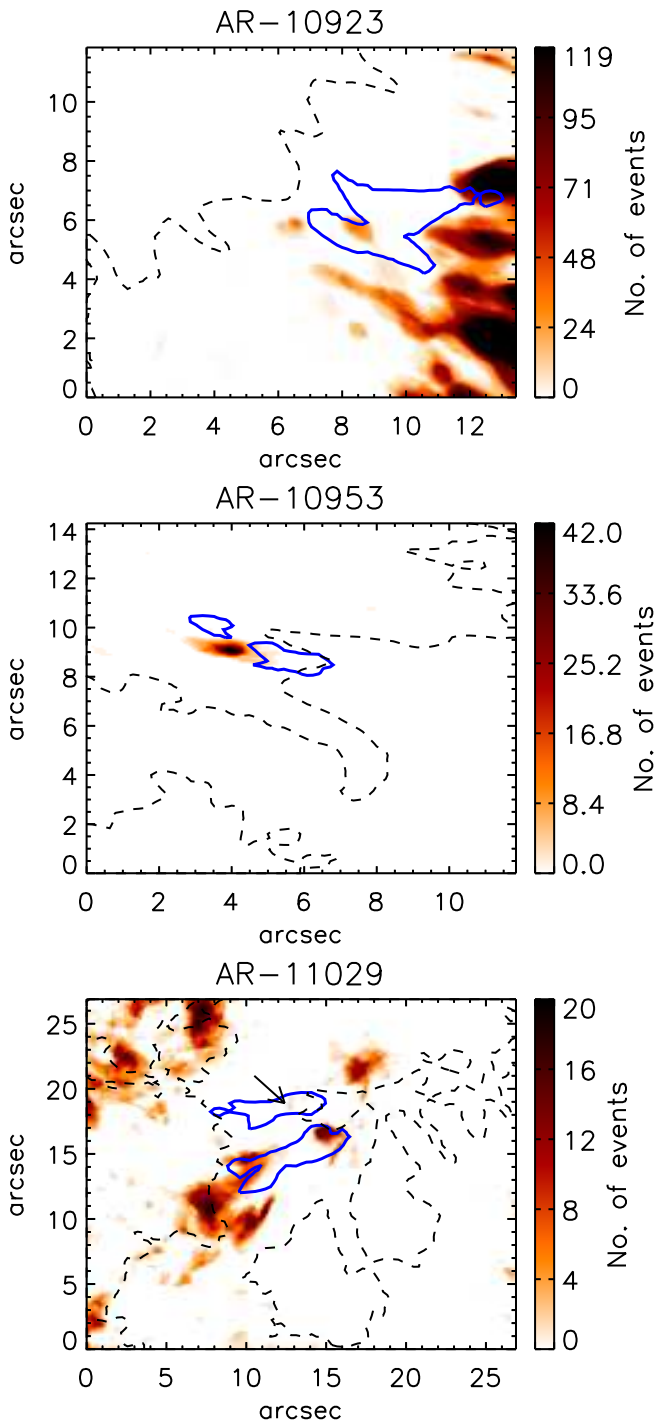


FIG. 8.— Ca event maps depicting locations with strong, persistent enhancements. The images have been scaled as shown by the vertical color bar. The black arrows indicate relatively short lived events. See text for details.

the 3 ARs. Figure 9 displays the G-band event maps derived using these threshold values. The strong, long lived chromospheric enhancements that were seen in AR 10923 are nearly co-spatial with G-band brightenings, although the sizes of the photospheric enhancements are relatively smaller than their chromospheric counterparts.

The G-band event map of AR 10953 consists of a single isolated blob close to the southern edge of the strong downflowing patch located near the umbra-penumbra boundary. This blob resembles a comet-like shape with the tail end protruding into the nearby light bridge. Rel-

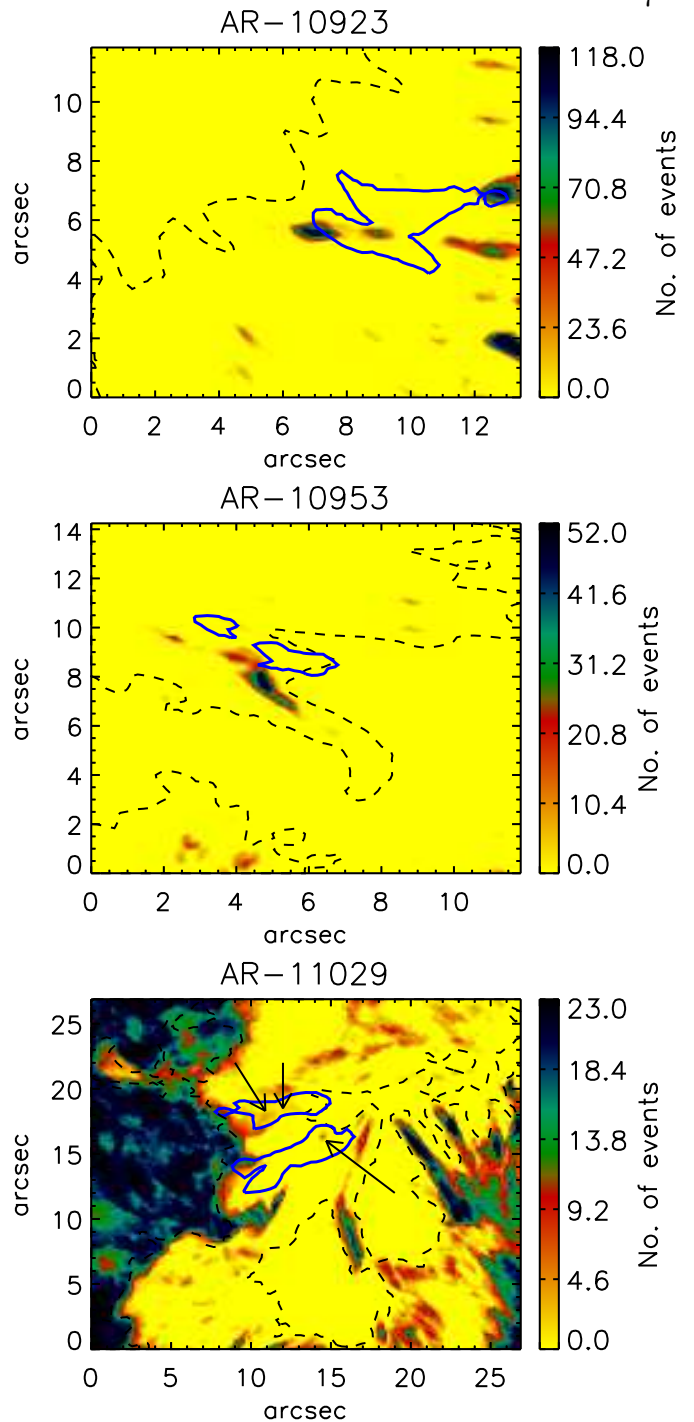


FIG. 9.— G-band event maps depicting locations with intensity close to the quiet Sun photosphere. The black arrows in the bottom panel indicate the few strong photospheric brightenings that lie within the downflowing patches.

atively fewer, though stronger events are also observed in between the two downflowing patches as well as close to the downflow area located furthest from the umbra-penumbra boundary.

In comparison to ARs 10923 and 10953, the photospheric event map of AR 11029 only shows traces of strong intensity in the downflowing areas at sporadic instances (see black arrows in the bottom panel of Figure 9.) If one assumes that the number of photospheric counts/events observed within the downflowing areas of AR 11029 occurred consecutively, the maximum lifetime

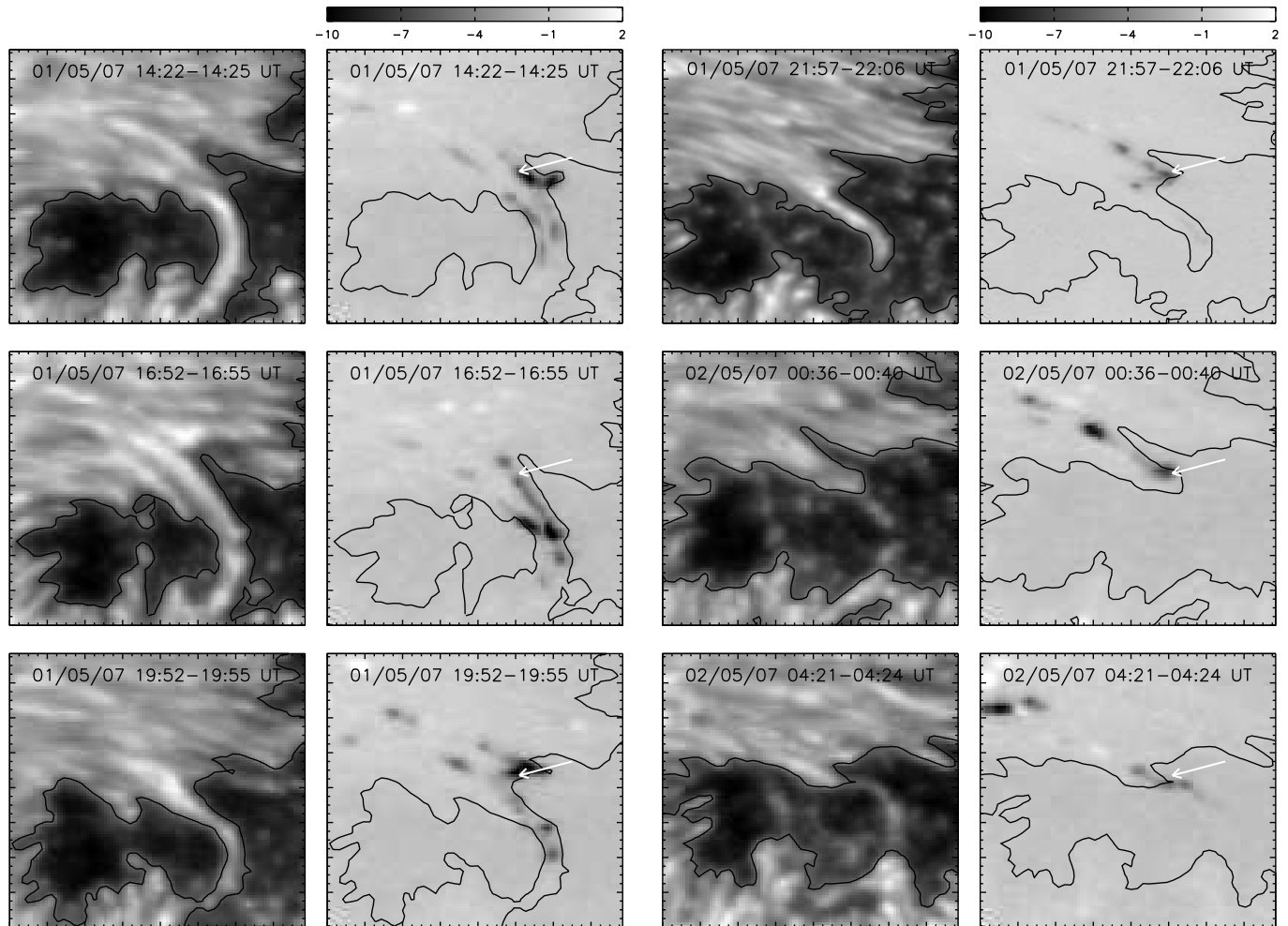


FIG. 10.— Temporal evolution of the strong downflows observed in AR 10953, with continuum images to the left and red wing magnetograms to the right. The date and time of the SP scan is indicated in each panel. All the magnetograms have been scaled identically and are given in per cent. The minimum value in the color bar has been clipped for better visibility of the downflowing regions. Each tickmark in the image corresponds to  $0''.5$ . The white arrow indicates a location corresponding to the downflows that was tracked in the magnetogram time sequence.

of these events would be equivalent to 35-40 minutes, since the filtergrams were acquired with a cadence of 5 min. In contrast, the lifetimes of similar brightenings in the other ARs is close to 1 hr.

The G-band event maps suggest that the process responsible for the supersonic downflows and the chromospheric enhancements is able to produce very strong brightenings in the photosphere that are nearly as intense as the quiet Sun but are also long lasting with lifetimes of up to 1 hr. Bright penumbral features close to the umbra-penumbra boundary with intensities nearly twice that of the quiet Sun have been detected by Denker et al. (2008) who speculate that these intermittent phenomena may be the outcome of reconnection between adjacent penumbral flux tubes.

#### 3.4. Temporal Evolution of the Downflows

In this section we study the evolution of the downflows in order to determine their lifetimes and to establish if they recur or change their position relative to the umbra-penumbra boundary. To that end, 5 additional data sets were selected for AR 10953 and 3 for AR 11029. AR 10923 is not considered here because only 2 more scans were available for analysis. All the observations were cal-

ibrated as explained in Section 2, constructing red wing magnetograms at 34.4 pm from the  $6302.5\text{\AA}$  line to identify the sites of strong downflows. In accordance with Figure 2, the sign of the red wing magnetogram has been reversed.

##### 3.4.1. NOAA AR 10953

The evolution of AR 10953 over the course of 14 hr from May 1 to May 2 is depicted in Figure 10. The continuum images and the red wing magnetograms were co-aligned with the scan taken at 21:57-22:06 UT with an accuracy of  $\pm 1$  pixel. The white arrow tracks the same downflowing region in time. The magnetogram signal at the position of the arrow is maximum ( $\sim 10\%$ ) during the first scan, taken at 14:22-14:25 UT. In the second scan the signal drops to nearly half this value before increasing to  $\sim 8\%$  at 19:52-19:55 UT. However, there are even stronger signals at the umbra-penumbra boundary where the amplitude of the magnetogram signal is  $\sim 12\%$ . This is nearly twice the signal detected in the next frame, which was analyzed earlier in Section 3.1.1. The scan made by the SP between 00:36-00:40 UT shows 3 isolated downflowing patches with one of them located at the umbra-penumbra boundary and a second stronger down-



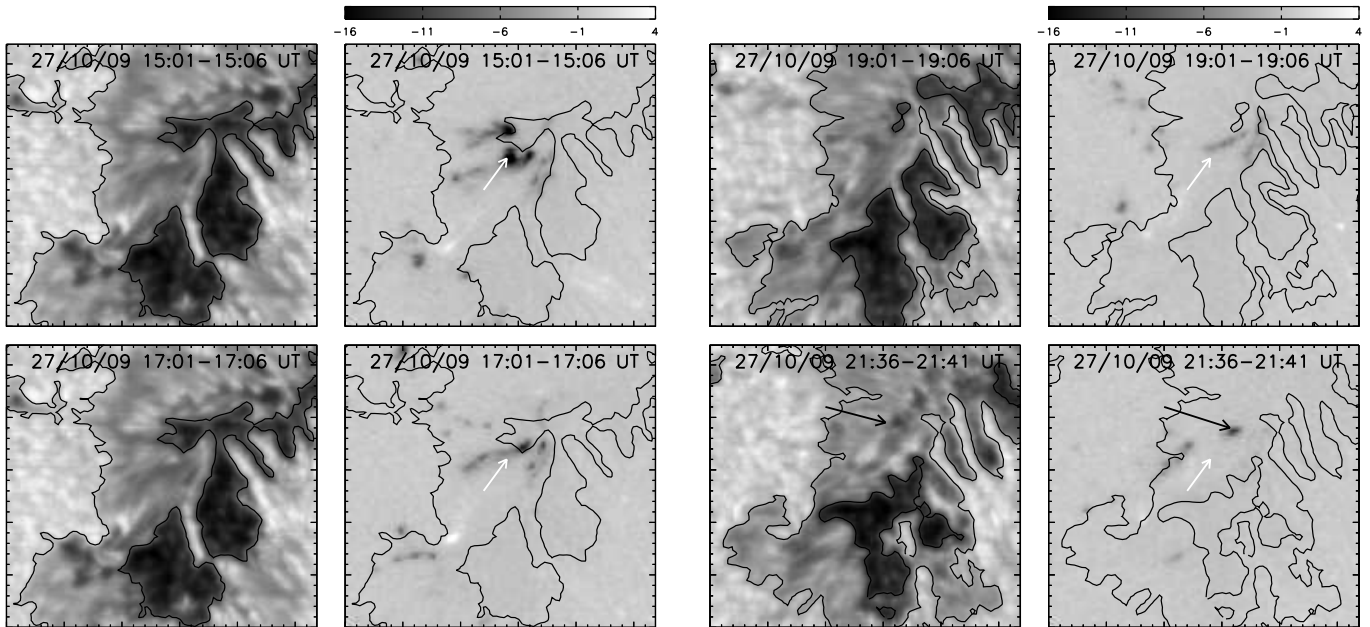


FIG. 11.— Same as Figure 10, for AR 11029. Each tickmark in the images corresponds to  $1''$ . The black arrow in the bottom panels indicate the location of the isolated downflowing patch close to the diffuse umbral fragment.

flow area  $5''$  away from the first. A third patch of downflows with much weaker signals is seen at a larger distance from the umbra-penumbra boundary. The last magnetogram, corresponding to 04:21-04:24 UT, shows diffuse signals of up to 5% at the umbra-penumbra boundary.

The time sequence of magnetograms illustrates the following: i) the strong downflows occurring at the umbra-penumbra boundary continue to be seen at this location in all 6 SP scans considered here, albeit with varying strength, which would put a lower limit of about 14 hr on their lifetimes; ii) the area of the strong downflowing patches at the umbra-penumbra boundary alone remains fairly constant ( $\sim 2 \text{ arcsec}^2$ ) during the latter half of the sequence from 21:57-04:24 UT.

### 3.4.2. NOAA AR 11029

The continuum images and the red wing magnetograms of AR 11029 were registered with the SP fast-mode map taken at 15:01-15:06 UT. The strong downflows observed at the umbra-penumbra boundary during this time interval (top right panel of Figure 11) can be seen in the following scan between 17:01-17:06 UT, nearly 2 hr later. The topmost downflowing zone is no longer visible, but the other velocity patch remains at the same location. This strong downflowing blob (indicated by the white arrow in the first scan) appears to rapidly ingress towards the umbra-penumbra boundary with a speed of some  $700 \text{ m s}^{-1}$ .

The scan taken between 19:01-19:06 UT demonstrates an intrusion of bright photospheric granules into the spot, with the umbra slowly being squeezed to occupy a much smaller area as depicted in the continuum image. The downflows continue to be observed near the shrinking umbral fragment. The scan made during 21:36-21:41 UT reveals a drastic shrinkage of the umbra with only a small area of strong downflows that appear close to where the umbra existed earlier (black arrow in the continuum image of Figure 11). In comparison to AR 10953, the

area of the downflowing patch near the umbra-penumbra boundary decreases with time. While the downflows occupy an area as large as  $6 \text{ arcsec}^2$  at 15:01 UT, this decreases to  $\approx 2.3 \text{ arcsec}^2$  by 21:36 UT. Common characteristics of the downflows observed in ARs 10953 and 11029 are their lifetimes of more than 6 hr and the fact that the long-lived ones appear to be located near the umbra-penumbra boundary. The more short-lived downflows are observed elsewhere in the ARs.

## 4. DISCUSSION

Supersonic downflows associated with the Evershed flow are usually observed in the outer penumbra (del Toro Iniesta et al. 2001; Bellot Rubio et al. 2004) or even beyond the sunspot boundary (Martínez Pillet et al. 2009). These downflows represent mass flux returning to the photosphere with a polarity opposite to that of the sunspot. As they are seen in the outer penumbra they cannot explain the strong downflows we have detected in the inner penumbra. One could suppose that the supersonic downflows near the umbra-penumbra boundary are the photospheric manifestations of some kind of inverse Evershed flow seen in the chromosphere. However, it is difficult to ascertain how such a chromospheric phenomenon could produce supersonic downflows in the inner penumbra at the photosphere.

Another mechanism that could perhaps explain the supersonic downflows is suggested below based on the orientation of the filaments in which they occur. The continuum images were morphologically *opened* (Curto et al. 2008) and subtracted from their original image in order to increase the contrast and isolate bright structures from the dark background, filament crossings, and diffuse edges. *Opening* is the result of two operations namely *erosion* followed by *dilation*. These two operators look for the neighborhood minimum and maximum where the search domain is defined by a structuring element (SE).

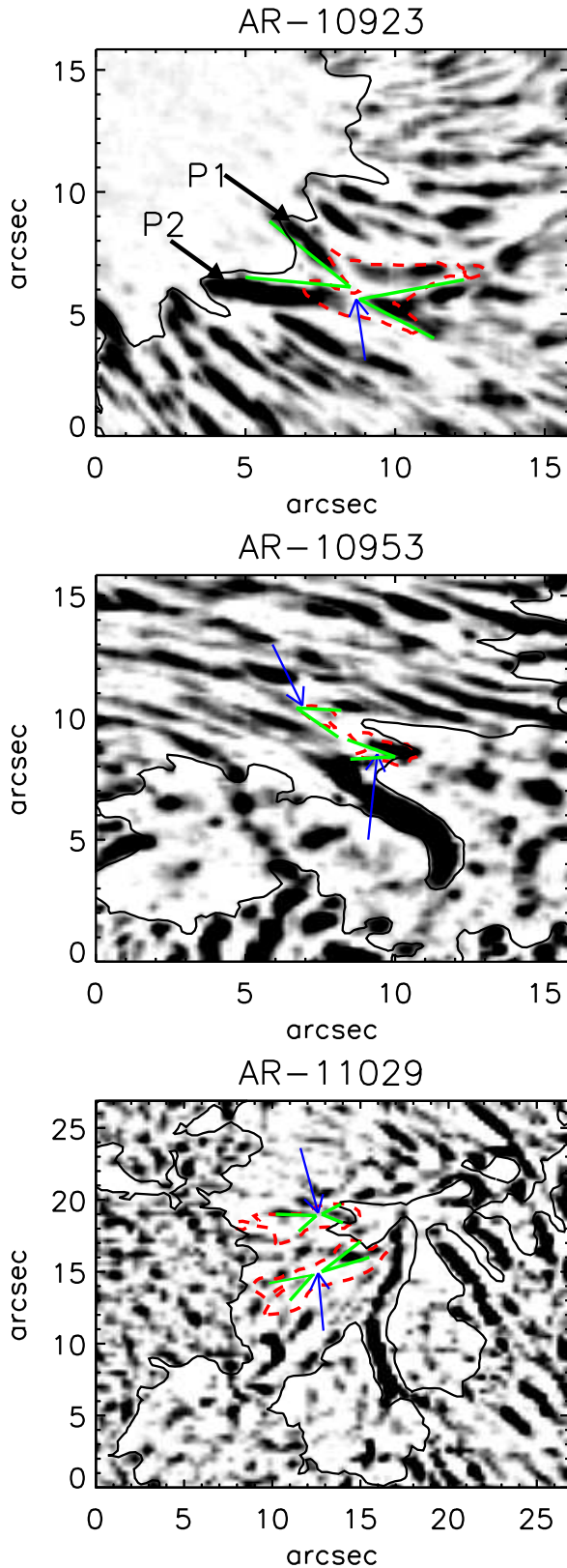


FIG. 12.— Morphologically *opened* images subtracted from the original image to separate bright filaments from the dark background, filament crossings, and edges. The images are shown in negative. The dark and bright structures correspond to the bright filaments and their diffuse counterparts, respectively. The blue arrows indicate locations where the filaments appear to intersect each other. P1 and P2 are the two intersecting filaments that were identified in NOAA AR 10923. The solid green lines refer to the bisecting angles between the filaments P1 and P2. The red dotted contour has been drawn for LOS velocities greater than  $2 \text{ km s}^{-1}$ .

The size of the SE used for *opening* the images was  $7 \times 7$  pixels for the first two ARs while a  $3 \times 3$  pixel SE was sufficient for AR 11029. The above morphological operation was chosen after discarding the Sobel and Roberts edge enhancement operator, unsharp masking, and intensity thresholding. The results are shown in Figure 12 with reversed signs. It is observed that in NOAA AR 10923, the strong downflows encompass two bisecting filaments P1 and P2 and their likely point of intersection is marked by a blue arrow. Such locations have been similarly marked for the other ARs, although they are less obvious. The orientation of the filaments resemble the post reconnection configuration illustrated in Figure 5c of Ryutova et al. (2008a), suggesting that the origin of the downflows is the slingshot effect associated with the reconnection of the filaments. The bisecting angles shown by the solid green lines in AR 10923 were estimated to be  $\approx 51^\circ$  and  $46^\circ$  respectively. In AR 10953 only one half of the intersecting filaments are visible, with the other end is possibly obscured by overlying filaments.

Ryutova et al. (2008a) identified several instances of filaments unwinding in a cork screw fashion leading to reconnection, transient brightenings and twists in the penumbral filaments. This model was proposed as a possible mechanism to explain the existence of MJJs. The magnetic configuration in the penumbra responsible for the MJJs was recently investigated by Magara (2010). According to this work, MJJs occur in the intermediate region between nearly horizontal flux tubes and the relatively vertical background field of the penumbra. A common aspect of both models is that only parts and not the entire penumbral filament participate in the reconnection, otherwise the filaments would be destroyed after several reconnection events.

We have detected chromospheric enhancements at the position of the strong downflows, although there is no strict one-to-one correspondence. In the downflowing regions or in their immediate vicinity there are also photospheric brightenings, with intensities nearly the same as the quiet Sun. This leads us to believe that a slingshot reconnection may be responsible for the chromospheric enhancements/jets, the photospheric brightenings, and the supersonic downflows. However, the physical process is different from those driving MJJs, since their lifetimes are much shorter than those of the events described here. While the lack of association of the strong downflows at the umbra-penumbra boundary with the Evershed flow is incontrovertible, the reconnection scenario has to be confirmed with simultaneous high-cadence spectropolarimetric scans of the photosphere.

## 5. SUMMARY

High resolution spectropolarimetric observations of 3 sunspots taken with *Hinode* indicate a new type of strong downflows in the inner penumbra. Such downflows are confined to isolated patches of  $1.5\text{--}6 \text{ arcsec}^2$  in area. The LOS velocities were estimated using the SIR inversion code, retrieving supersonic or nearly supersonic values from  $5 \text{ km s}^{-1}$  to  $10 \text{ km s}^{-1}$  in the downflowing patches of all three ARs. The velocity patches occur very close to or at the umbra-penumbra boundary, which makes them the largest velocities ever detected at these locations in a sunspot. Shimizu et al. (2008), on the other hand, reported frequent instances of supersonic downflows at the

border of an umbra without a penumbra.

The strong velocities are usually associated with magnetic fields of more than 2 kG having the same polarity as the sunspot. This implies that the downflows are not driven by the Evershed flow, although the latter could independently be present at those locations. Intense and long lived chromospheric brightenings are seen near the strong photospheric downflows extending over an area of  $\approx 1\text{--}2 \text{ arcsec}^2$ . Photospheric brightenings nearly as intense as the quiet Sun are also present in the downflowing regions or close to them. They are persistent as their chromospheric counterparts. In addition, the downflows may have lifetimes of up to 14 hr (or more) as can be judged from several consecutive Hinode/SP scans.

The strong downflows are associated with penumbral filaments that appear to be twisted in the manner described by Ryutova et al. (2008b) that would arise from a reconnection process. Such a process is believed to produce the transient penumbral microjets. Microjets occur everywhere in the penumbra and the photospheric downflows observed with them are typically  $1 \text{ km s}^{-1}$ , as reported by Katsukawa & Jurčák (2010). The chromospheric brightenings described in Section 3.2 however, are more intense, long lived and bigger than the microjets but neither as intense nor intermittent as a flare.

The long-lived downflows reported here are not observed in all ARs as is evident from an inspection of the

Level 1 SP maps<sup>3</sup> from 2006 Nov to 2010 Feb. Although a total of 120 ARs were indexed by NOAA during this period, only 3 additional candidates were identified to show strong downflows lasting 2 or 3 consecutive scans. These include AR 10956 on 2007 May 16, AR 10978 on 2007 Dec 12 and AR 10988 on 2008 April 1.

The strong photospheric downflows that we have described in this paper have not been reported earlier and as such represent a new phenomenon. They are possibly driven by dynamic processes occurring in the inner penumbra which affect the chromosphere as well. The lack of a suitable theory for these events poses a challenge for future numerical simulations of sunspots.

Our sincere thanks to the *Hinode* team for providing the data used in this paper and the referee for his/her comments. *Hinode* is a Japanese mission developed and launched by ISAS/JAXA, with NAOJ as domestic partner and NASA and STFC (UK) as international partners. It is operated by these agencies in co-operation with ESA and NSC (Norway). Financial support by the Spanish Ministerio de Ciencia e Innovación through project AYA2009-14105-C06-06 as well as PCI2006-A7-0624 and by Junta de Andalucía through project P07-TEP-2687 is gratefully acknowledged.

<sup>3</sup> See <http://www.lmsal.com/solarsoft/data/hinode/sot/level1d>

#### REFERENCES

- Bellot Rubio, L. R., Balthasar, H., Collados, M. 2004, *A&A*, 427, 319
- Bellot Rubio, L. R., Schlichenmaier, R., Tritschler, A. 2006, *A&A*, 453, 1117
- Bellot Rubio, L. R., Tsuneta, S., Ichimoto, K., Katsukawa, Y., Lites, B. W., Nagata, S., Shimizu, T., Shine, R. A., Suematsu, Y., Tarbell, T. D., Title, A. M., del Toro Iniesta, J. C. 2007, *ApJ*, 668, L91
- Borrero, J. M., Lagg, A., Solanki, S. K., Collados, M. 2005, *A&A*, 436, 333
- Cabrera Solana, D., Bellot Rubio, L. R., Beck, C., del Toro Iniesta, J. C. 2007, *A&A*, 475, 1067
- Curto, J. J., Blanca, M., Martínez, E. 2008, *Sol. Phys.*, 250, 411
- del Toro Iniesta, J. C., Bellot Rubio, L. R., Collados, M. 2001, *ApJ*, 549, L139
- Denker, C., Tritschler, A., Deng, N. 2008, *AN*, 329, 773
- Evershed, J., 1909, *MNRAS*, 69, 454
- Franz, M., Schlichenmaier, R. 2009, *A&A*, 508, 1453
- Ichimoto, K., Shine, R. A., Lites, B., Kubo, M., Shimizu, T., Suematsu, Y., Tsuneta, S., Katsukawa, Y., Tarbell, T. D., Title, A. M., Nagata, S., Yokoyama, T., Shimojo, M. 2007, *PASJ*, 59, S593
- Ichimoto, K., et al. 2008, *Sol. Phys.*, 249, 233
- Katsukawa Y., Berger, T., Ichimoto, K., Lites, B. W., Nagata, S., Shimizu, T., Shine R. A., Suematsu, Y., Tarbell, T. D., Title, A. M., Tsuneta, S. 2007, *Science*, 318, 1594
- Katsukawa, Y., Jurčák, J. 2010, *A&A*, 524, 30
- Kosugi, T., et al. 2007, *Sol. Phys.*, 243, 3
- Lites, Q. W., Elmore, D. F., Streander, K. V. 2001, *ASP Conf. Series*, 236, 33
- Louis, R. E., Bayanna, A. R., Mathew, S. K., Venkatakrishnan, P., 2008, *Sol. Phys.*, 252, 43
- Louis, R. E., Bellot Rubio, L. R., Mathew, S. K., Venkatakrishnan, P., 2009, *ApJ*, 704, L29
- Magara, T. 2010, *ApJ*, 715, L40
- Martínez Pillet, V., Katsukawa, Y., Puschmann, K. G., Ruiz Cobo, B. 2009, *ApJ*, 701, L79
- Mathew, S. K., Lagg, A., Solanki, S. K., Collados, M., Borrero, J. M., Berdyugina, S., Krupp, N., Woch, J., Frutiger, C. 2003, *A&A*, 410, 695
- Rimmele, T. R. 1994, *A&A*, 290, 972
- Rimmele, T. R., & Marino, J. 2006, *ApJ*, 646, 593
- Roupe van der Voort, L. H. M. 2003, *A&A*, 397, 757
- Ruiz Cobo, B., Del Toro Iniesta, J. C. 1992 *ApJ*, 398, 375
- Ryutova, M., Berger, T., Frank, Z., Title, A. 2008a, *ApJ*, 686, 1404
- Ryutova, M., Berger, T., Title, A. 2008b, *ApJ*, 676, 1356
- Sainz Dalda, A., Bellot Rubio, L. R. 2008, *A&A*, 481, L21
- Schlichenmaier, R., Schmidt, W. 1999, *A&A*, 349, L37
- Shimizu, T., Lites, B. W., Katsukawa, Y., Ichimoto, K., Suematsu, Y., Tsuneta, S., Nagata, S., Kubo, M., Shine, R. A., Tarbell, T. D. 2008, *ApJ*, 680, 1467
- Shimizu, T., Katsukawa, Y., Kubo, M., Lites, B. W., Ichimoto, K., Suematsu, Y., Tsuneta, S., Nagata, S., Shine, R. A., Tarbell, T. D. 2009, *ApJ*, 696, L66
- Shine, R. A., Title, A. M., Tarbell, T. D., Smith, K., Frank, Z. A., Scharmer, G. 1994, *ApJ*, 430, 413
- Solanki, Sami K. 2003, *A&A Rev.*, 11, 153
- Tsuneta, S., et al. 2008, *Sol. Phys.*, 249, 167
- Westendorp Plaza, C., del Toro Iniesta, J. C., Ruiz Cobo, B., Martínez Pillet, V., Lites, B. W., Skumanich, A. 1997, *Nature*, 389, 47